Structure−Phase State and Properties of Al−Cu−Fe Quasi-Crystalline HVAF Coating Produced from Water-Atomized Powder

Tian Haoliang, Wang Changliang, Li Zhang, M. O. Iefimov[*],
N. P. Zakharova[*], and V. A. Goncharuk[*]

Aviation Key Laboratory of Science and Technology
on Advanced Corrosion and Protection for Aviation Material Beijing,
Beijing Institute of Aeronautical Materials,
CN-100095 Beijing, China
[*]I. M. Frantsevich Institute for Problems in Materials Science, N.A.S. of Ukraine,
3 Academician Krzhyzhanovsky Str.,
UA-03142 Kyiv, Ukraine

High-velocity air fuel (HVAF) spraying is used to produce an Al−Cu−Fe quasi-crystalline (QC) coating from a water-atomized powder on a low-carbon steel (A284Gr.D/SS330). As shown, HVAF method shows a good efficiency in the production of protective coatings with acceptable porosity, needed thickness, sufficiently high mechanical characteristics, and anti-corrosion properties. As shown, HVAF process allows controlling the volume fraction of $Al_{63}Cu_{25}Fe_{12}$ quasi-crystalline phase in the produced coating. The produced QC coating possesses a high cohesion strength ($\cong 565$ MPa) and good adhesion to the steel substrate providing avoidance of the coating detachment at bending. As shown, the $Al_{63}Cu_{25}Fe_{12}$ quasi-crystalline coating has satisfactory resistance and hindered formation of surface corrosion damage in artificial sea water due to the formation of a passivating oxide film based on aluminium oxide.

Key words: Al−Cu−Fe quasi-crystal, mechanical properties, coating, high-velocity oxygen fuel spraying, water-atomized powder.

Високошвидкісне повітряно-паливне (HVAF) напорошування використа-

Corresponding author: Nataliya Petrivna Zakharova
E-mail: Zah@ipms.kiev.ua

но для одержання квазикристалічного покриття Al−Cu−Fe з розпороше-
ного водою порошку на низьковуглецевій криці (сталь Ст3). Показана хо-
роша ефективність методи HVAF у виробництві захисних покриттів з
прийнятною поруватістю, необхідною товщиною, достатньо високими
механічними характеристиками та антикорозійними властивостями. По-
казано, що процес HVAF дає змогу контролювати об'ємну частку квази-
кристалічної фази $Al_{63}Cu_{25}Fe_{12}$ у виготовленому покритті. Одержане ква-
зикристалічне покриття має високу когезійну міцність ($\cong 565$ МПа) і хо-
рошу адгезію до крицевої основи, що дає змогу уникнути відшарування
покриття за випробувань на вигин. Показано, що квазикристалічне пок-
риття $Al_{63}Cu_{25}Fe_{12}$ має задовільну стійкість до утворення поверхневих ко-
розійних пошкоджень у штучній морській воді завдяки утворенню паси-
вувальної оксидної плівки на основі оксиду алюмінію.

Ключові слова: квазикристал Al−Cu−Fe, механічні властивості, покрит-
тя, високошвидкісне повітряно-паливне напорошування, розпилений во-
дою порошок.

1. INTRODUCTION

Metallic materials with a quasi-crystalline atomic structure are char-
acterized by a number of unique properties, namely high hardness,
stiffness, wear resistance, and thermal barrier properties, which are of
great interest to researchers in the point view of possible industrial
application [1−3]. However, very low fracture toughness K_{1C} [4] causes
rather low plasticity and thus brittleness of quasi-crystals at room
temperature, which limit the possibility of obtaining the final prod-
ucts from quasi-crystalline (QC) materials by plastic deformation.
Hardness and fracture toughness measurements, for example, have
been performed by means of indentation technique on the decagonal
Al−Cu−Co−Si and the icosahedral Al−Cu−Li, Al−Cu−Fe, Al−Fe−Cr
quasi-crystals [2−6].

At the same time, a number of recent works are devoted to the re-
search of composite protective layers strengthened by quasi-
crystalline particles, which demonstrate increased operational charac-
teristics. This applies both to the so-called natural composites contain-
ing QC particles [6], and to artificially manufactured layers of compo-
site strengthened by QC particles during severe plastic deformation of
the matrix material surface [7−12]. However, such protective compo-
site layers may only be effective in providing sufficient wear re-
sistance, but are less suitable for the surfaces operating in aggressive
environments and thus subjected to corrosion attack.

Another approach, which is based on the formation of protective
coatings with a QC structure, may be more promising, as it simultane-

ously provides increased resistance to corrosion and wear [13, 14]. However, the specified operational characteristics largely depend on a number of parameters of the resulting coating, such as the coating thickness, porosity, adhesion, as well as physical and mechanical properties, which, in turn, depend on the production method of the protective coating.

The literature survey shows that a number of atomic deposition methods are currently used to obtain QC coatings, including thermal spraying [13, 14], air plasma spraying [15] magnetron sputtering [16, 17], electron beam (EB) PVD technique [18,19], *etc*. The listed methods make it possible to form coatings of different thickness, structural phase state and properties.

Recently, one of the most promising approaches are the methods that use a pre-made powder of a given composition and structural phase state. For instance, for the manufacturing of the 3*D*-built products, laser or electron beams are frequently used in laser powder bed fusion (L-PBF), selective laser melting (SLM), or electron beam melting (EBM) techniques.

Quasi-crystalline powders were reported can be produced by mechanical milling [20, 21], gas-atomization [7], and/or water atomization [22–24]. The sequence of solid-state phase transformations in high-energy ball-milled Al–Cu–Fe alloy powders upon constant-rate heating were examined by in situ synchrotron radiation diffraction and thermal analysis (DSC/DTA) methods. The as-milled Al–Cu–Fe nanopowders were consolidated into disk-shape pellets using field-activated spark-plasma sintering (FAST/SPS) [25]. It was also reported that gas-atomized powders of an Al–2.6Cr–1.6Co–1.5Mn–0.5Zr alloy (at.%) exhibited a nano-composite microstructure consisting of a face cantered cubic (f.c.c.) Al matrix with $\approx 35\%$ by volume of icosahedral quasi-crystalline dispersoids. Powders of three more dilute Al–Cr–Mn–Co–Zr alloys were studied in [26]. As shown, the same main phases (f.c.c. Al and I phase) were produced in these three alloys, but that the size, morphology, and distribution of the I-phase vary significantly with both the alloy composition and the cooling rate, *i.e.,* with the powder particle size. A water-atomization method was developed in IPMS, NAS of Ukraine [22]. It was shown that QC powders and QC containing powders of various systems (Al–Cu–Fe, Al–Fe–Ti–Cr) can be obtained.

Accounting for some limitations for QC powder remelting or heating up to the temperature higher than some critical one, a high-velocity air-fuel (HVAF) technique can be considered as a prospective method for QC coating production. This method allows controlling the temperature applied during the deposition process, and this feature permits producing the coatings with different contents of QC phase starting from the QC powder.

This work aims to characterize the quasi-crystalline $Al_{63}Cu_{25}Fe_{12}$ coating produced by HVAF method. The coating microstructure and phase state, porosity, hardness, and cohesion/adhesion are particularly assessed for the coating obtained by the optimized HVAF regime.

2. EXPERIMENTAL DETAILS

To produce a quasi-crystalline coating, powders of the Al−Cu−Fe system obtained by spraying the melt with a high-pressure water jet were used [22, 24]. The melt was prepared from A5 aluminium (99.95%), cathode copper (99.99%), and Armco iron (99.92%). Estimates of the cooling rate of powders for this type of production gives 10^6 K/s [22]. The SEM image of the powders is shown in Fig. 1, and their size distribution is shown in Table 1. To obtain coatings, powders with a size ranges 40−80 μm were used. The use of special inhibitors makes it possible to almost completely eliminate the oxidation of powders.

Coatings were deposited on a low-carbon steel (Ст3/A284Gr.D/SS330) substrate by the HVAF spraying method, which is successfully used to obtain heat- and wear-resistant metal and composite coatings [27]. To provide higher adhesion, the shot peening treatment was performed prior the HVAF deposition to form a clean and rough enough substrate surface. Coatings were applied to samples in the form of disks 25.4 mm in diameter and 10 mm high (coating thickness was 225 ± 25 μm), as well as stripes $100{\times}25{\times}2$ mm in size (coating thickness was 100−125 μm).

The phase composition of the water-atomized powders and produced coatings was controlled by x-ray diffraction analysis using a DART-UM1 diffractometer in CuK_α irradiation. The amount of the icosahedral QC phase was determined in accordance with the calibration curve proposed in [14] (correlation of the phase structure with the intensity of x-ray maxima from the quasi-crystalline and b.c.c. β-phases). The structure of the resulting coatings was monitored by scanning electron
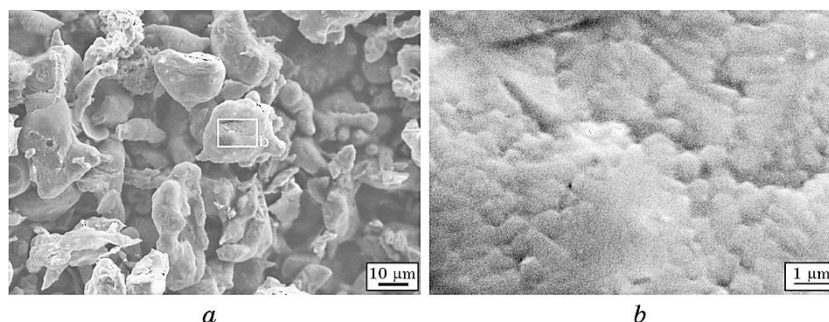

Fig. 1. SEM images of the water-atomized powder $Al_{63}Cu_{25}Fe_{12}$.

TABLE 1. Size distribution and chemical composition of the water-atomized QC powder used for production of QC Al–Cu–Fe coating.

Obtained powder		Chemical composition, % wt./at.%			
Particle size μm	Volume fraction, %	Al	Cu	Fe	O
−40	7.5	42.4/62.6	39.6/24.7	17.8/12.6	0.2/0.5
−80+40	50	42.5/62.3	40.3/25.1	17.0/12.1	0.2/1.2
−100+80	13.5	42.1/62.0	40.2/25.2	17.5/12.4	0.18/0.45
+100	29	–	–	–	–

microscopy (SEM) (using a Superbrobe microscope). The porosity of the resulting coatings was evaluated using optical microscopy (Neophot 32) using the secant method, as well as using ImagePro software for the image analysis.

The microhardness of the produced QC coatings before and after annealing was measured using a PMT-3 device with a load of 100 g on a Vickers diamond indenter. The hardness values were averages on the base of 10−15 measurements.
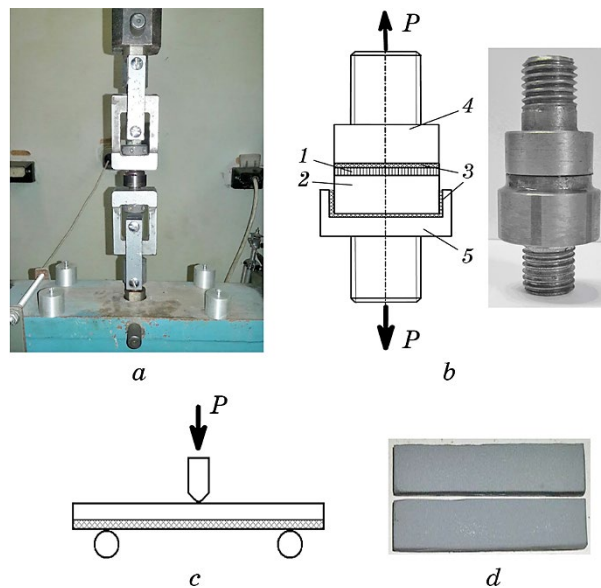
Fig. 2. The upper (fixed) and lower (movable) grips of the P-5 tensile machine (*a*), scheme and photo of the sample tested for assessment of the adhesion strength (*b*), scheme for three-point bending test (*c*), and view of the bend samples with QC coating (*d*). *P* is the load.

The disc-shaped specimens were used to assess the adhesive strength of the 'coating-substrate' complex samples through the tensile tests on a R-5 testing machine (Fig. 2, *a*). The fastening of the sample was carried out by gluing the coated sample between the punches (Fig. 2, *b*), which, in turn, were fastened with threads in the upper (fixed) and lower (movable) grips. Adhesion was determined using the formula: $\sigma = P_{max}/S$, where $S = \pi d^2/4$ is the area of the coated surface, P_{max} is the maximum tensile force.

Additionally, the adhesive strength of the coating-substrate pair was assessed by using the three-point bending tests, the test base was 23 mm (Fig. 2, *c*). Samples in the form of strips with QC coating were used. The moving gripper speed was 0.25 mm/min. During mechanical testing of both types, the loading curves were recorded in the 'load–displacement' coordinates.

Assessment of the corrosion resistance was performed on the base of visual analysis of the coating surface after holding in the artificial sea water (3% NaCl) for various times (up to 10 days). Metallographic microscope Neophot 32 was used to reveal any corrosion damage after holding in aggressive medium.

3. RESULTS AND DISCUSSION

Figure 3 shows the SEM images of the surface topography (Fig. 3, *f*) and cross-section appearance (Fig. 3, *b*) of the QC coating produced on the Steel Ст3 substrate. It is seen that the powder particles appear as deformed plates of irregular shape after the HVAF spraying. The surface integrity is high enough since no visible cracks and/or defects are visible. The surface roughness is seen to be not very high. The formed surface volleys are broad and shallow, *i.e.*, the maximum surface


a   *b*
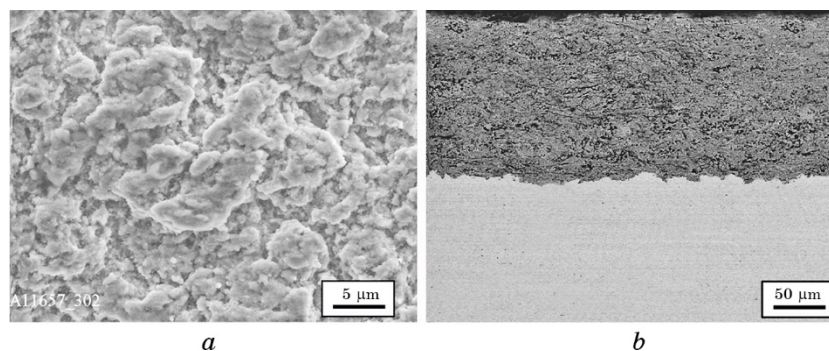
Fig. 3. SEM images of the surface morphology (*a*) and cross-section (*b*) of the $Al_{63}Cu_{25}Fe_{12}$ HVAF-coating produced on the substrate made of low-carbon steel.
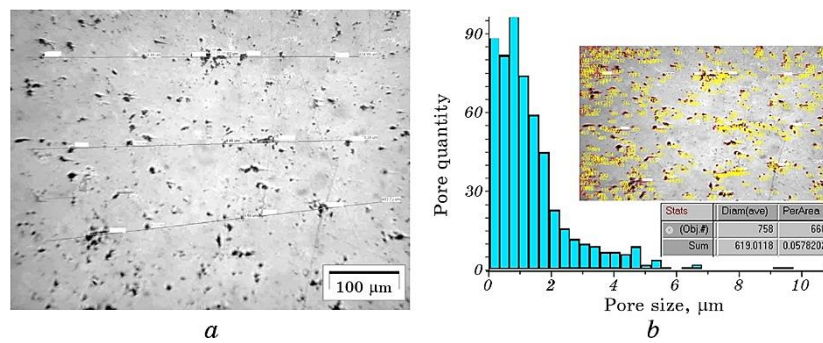
Fig. 4. Examples of the measurements of the porosity of QC coating on low-carbon steel substrate using a secant method (*a*) and analysis by the computer-aided ImagePro software (*b*). Evaluated porosity is about 6%.

roughness R_t is relatively low and the average spacing of adjacent peaks in the surface roughness profile D_p is large. It thus can be considered that the stress concentration factor $K_t = 1 + 4(R_t/D_p)^{1.3} = 1.103$ ($R_t \approx 7.2\,\mu m$, $D_p \approx 120\,\mu m$) is well allowable in the sense of the avoid of probable deterioration of the overall properties of the coating. Similar stress concentration factor was reported for the Ni-based HVAF coating ($K_t \approx 1.089$) [27], while it even lower than that assessed for the surface formed by the electric discharge surface alloying ($K_t \approx 1.17$) [28].

The thickness of the formed QC coating is about 100–130 μm (Fig. 3, *b*). The transition zone between the coating and the steel substrate can supply a good adhesion because of the purposely performed shot peening treatment prior the HVAF spraying. Such preparative shot peen-
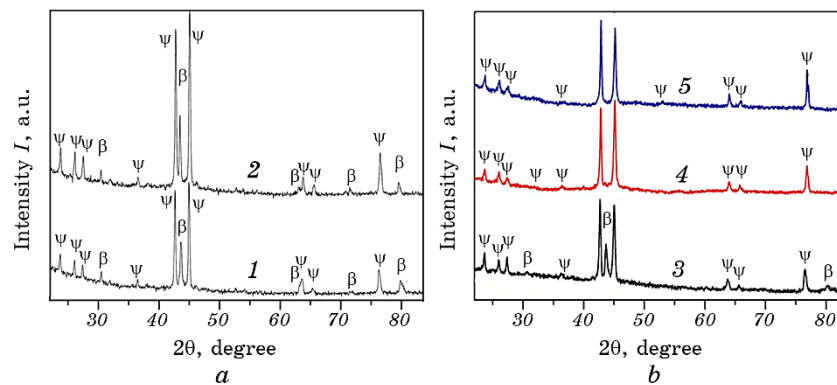
Fig. 5. X-ray patterns from the water-atomized $Al_{63}Cu_{25}Fe_{12}$ powder (75% QC) (*1*), from the $Al_{63}Cu_{25}Fe_{12}$ coating (*2*) deposited on a substrate from steel Ст3 (*a*) and after annealing at 400°C for 60 min (*3*), 725°C for 20 min (*4*) and 725°C for 60 min (*5*) (*b*).
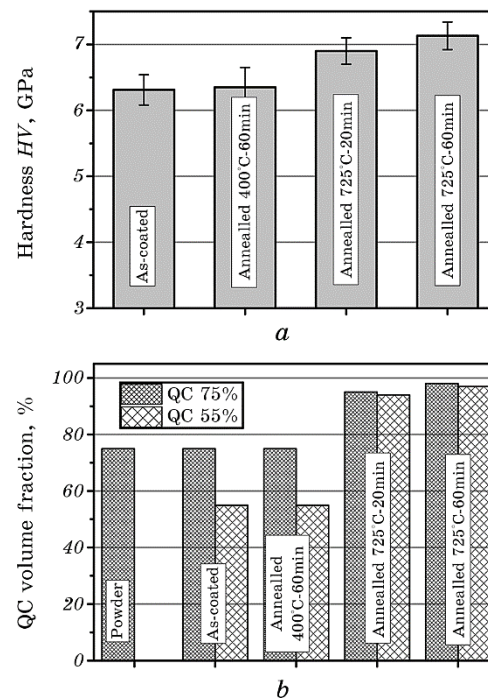
Fig. 6. Dependence of microhardness *HV* (*a*) and phase composition (*b*) of the Al−Cu−Fe QC coating on the heat-treatment regime.

ing provides appearance of some irregularities that further play a role of specific sites of coupling (Fig. 3, *b*).

One of the important characteristics of the resulting coatings is their porosity. Usually, the pore sizes ranges in a fairly wide interval. Figure 4 shows the outcomes of the application of two methods for measuring porosity of the coatings deposited on the steel Ст3 substrate: a secant method (Fig. 4, *a*) and analysis by the computer-aided ImagePro software (Fig. 4, *b*).

Both methods lead to similar results—porosity of the formed QC coating was assessed to be $\cong 6-7\%$ (a secant method) and 5.78% (ImagePro). The latter analysis allows considering the size and quantity of the observed pores (see histogram in Fig. 4, *b*) as well as their shape characteristics of various types (not shown). A vast majority of the pores are lower than 2 μm in size, while some portion of slightly lager pores is also observed. Nevertheless, analysis of the average pore size allows expecting their low influence on the mechanical properties of the coating. Additional annealing at 400°C was also used to perform the relaxation of residual stress formed in the coating during the HVAF-induced warm deformation of the water-atomized powder fol-

lowed by natural cooling.

Determination of the volume fraction of QC phase in both the water-atomized powder and the HVAF produced coating was performed using the XRD data and a calibration graph suggested by Sordelet [14] that established the correlation between the intensity of appropriate XRD peaks and the volume fractions of the QC and beta- phases in the Al–Cu–Fe samples. Naturally, the volume fraction of QC phase in the analysed coating may vary dependently on the HVAF regime. In this study, the HVAF spraying regime used allowed to sustained the volume fraction of QC phase to be 75% wt. (Fig. 5, *a*). However, a few coatings were produced with some overheating during the HVAF spraying process resulting in the 50–55% wt. content of QC phase in the coating to examine of the effects of further thermal treatments on the phase composition.

XRD data shown in Figure 5, *a* confirm that the used HVAF spraying regime allows obtaining the coating with the same content of the QC phase in comparison with that in the water-atomized powder. The effects of thermal treatments were studied for two temperatures, namely 400°C and 725°C. The first heat treatment (at 400°C) is only providing some stress-relieving effect on the HVAF coating, which manifests itself by slight increase in the microhardness of the QC coating (Fig. 6, *a*). Additionally, the coatings were annealed at 725°C for various durations. In accordance with the Al–Cu–Fe phase diagram [29], this temperature is just beneath the critical upper temperature limiting the existence of the QC phase. Measurements show that after this annealing at 725°C for 20 and 60 min, microhardness of the coating increases to 6.9 GPa and 7.13 GPa, respectively (Fig. 6, *a*). XRD
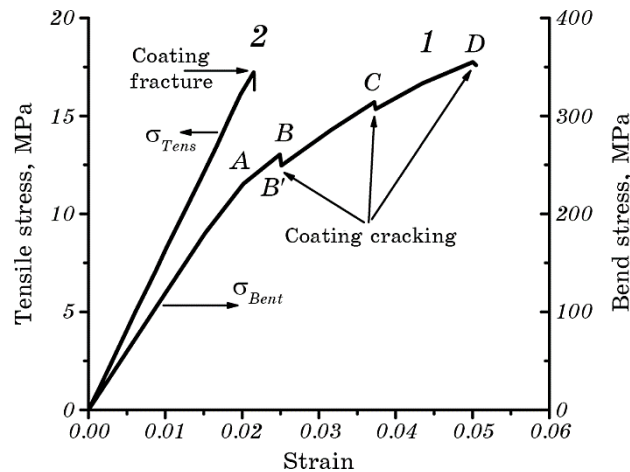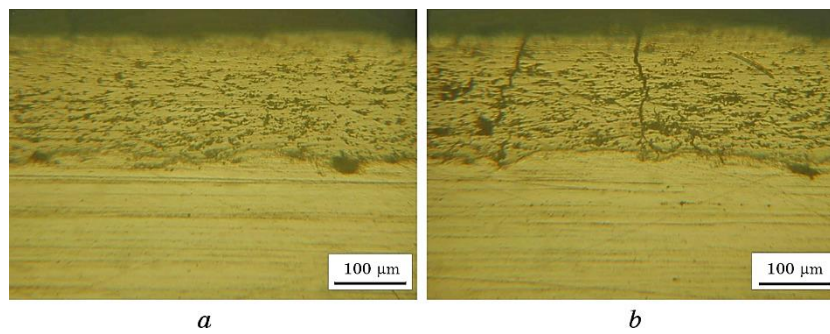

Fig. 7. Loading diagrams for the 'Al–Cu–Fe coating–substrate' complex specimen at bending test (*1*) and Al–Cu–Fe coating at tensile (adhesion) tests (*2*).

Fig. 8. Optical images of 'Al–Cu–Fe coating–substrate' complex specimen before (*a*) and after (*b*) three-point bend testing. Arrows indicate the cracks formed in the coating normally to the substrate surface.

data shows that the coating undergoes the transition from QC + beta two-phase state to mono-phase QC state after holding at 725°C for 20 min. Further holding at this temperature does not effect on the phase composition, but slightly increase the microhardness.

The results of an experimental study of the strength of the quasi-crystalline 'QC coating–steel substrate' (sample hereafter) system are shown in Fig. 5, and the nature of crack propagation in the coating and substrate at different loading stages is shown in Fig. 6. Tests have shown that several areas can be distinguished on the load diagrams, which correspond to separate stages of deformation and destruction of the sample (the beginning and end of the regions are indicated by letters).

The stress-strain diagram registered during bending (Figure 7) shows that from the beginning of loading to point A, corresponding to the yield strength of the steel substrate, the sample is elastically deformed without a noticeable discontinuity of the coating and substrate. After point A, plastic deformation of the substrate material begins $\sigma_{Ys} = 231$ MPa. The presence of the coating does not significantly affect the curve in section $A–B$ due to its small thickness compared to the thickness of the steel substrate. In the $B–B'$ interval, a significant stress drop occurs (from 260 to 249 MPa), due to the initiation and propagation of a crack. Repeatedly, the process of formation of a crack in the coating occurs near points C and D, but with a much smaller load drop. Further exposure was stopped to determine the relationship between adhesion and cohesion characteristics of the coating.

Microscopic examination of the cross-section of the coating after bending tests showed that flexural failure occurs perpendicular to the substrate, earlier than the detachment of the coating begins (Fig. 8, *b*). Thus, the adhesion strength of the 'coating–substrate' pair is higher than the cohesive strength of the QC coating itself. In addition, the

TABLE 2. Adhesion of the Al–Cu–Fe QC coating on low-carbon steel.

Test method	QC V_f, %	Sample state	Adhesion, MPa
Bent tests	75	As-coated	>
Tensile test	75	As-coated	8.1
		Annealing at 400°C for 60 min	7.4
	50–55	As-coated	16.7
		Annealing at 400°C for 60 min	15.5

quasi-crystalline coating is sufficiently strong and withstands stresses in the region of elastic deformation of the substrate before the substrate begins to flow. The destruction of the coating occurs almost immediately after the start of the flow of the substrate material. The deformation transferred from the plastic matrix to the elastic coating after reaching the yield point, but not leading to cracking in the coating, is $e = 0.003$.

The cohesive strength of the coating can be estimated [30] by the sum $\sigma_{Ys} + \Delta\sigma$, where σ_{Ys} is the yield strength of the substrate, and $\Delta\sigma = Ee$ is the increase in elastic stresses in the coating. To estimate this increase, it is necessary to know the value of the elasticity modulus QC of the coating E. However, various authors report different values of elastic modulus for QC of Al–Cu–Fe system. If we take the coverage modulus $\cong 100$ GPa [30], then the value of $\Delta\sigma$ can be estimated as 300 MPa. If we would follow Ref. [5], then the elastic modulus for icosahedral QC of Al–Cu–Fe would be 171 GPa, and thus $\Delta\sigma$ would be 513 MPa. According to the calculations from the melting temperatures, $E = 110$ GPa and $\Delta\sigma = 330$ MPa [4]. Therefore, dependently on the elastic modulus for Al–Cu–Fe QC used the cohesion strength of the coating would be different. Based on the magnitude obtained from the calculations [4] and experimentally observed strain ($e = 0.003$) the cohesion strength (565 MPa) would be very close to the similar estimation (560 MPa) obtained for QC coating on the 5056-aluminum alloy substrate in [30]. Relatively high cohesion is seemingly related to the irregular surface of the particles of the water-atomized QC powder (Fig. 1, *b*), which provides additional coupling sites and so-called 'cold welding' of the powder particles during plastic deformation induced by the collisions of the particles flight particles by the substrate surface at HVAF process.

To assess the adhesion of the QC coating to the steel substrate the tensile tests were performed using the clue fabricated samples (see Fig. 2, *b*). Example of the registered tensile curve is shown in Fig. 7 (curve

2). It demonstrates that during tensile loading the tested sample underwent only elastic deformation and fractured at a certain stress related to the coating cohesion strength and residual porosity of the coating, which might slightly decrease the real area of the tensile sample. The registered adhesion characteristics are listed in Table 2 for the tested coatings with various volume fractions of the QC phase and various states (as-coated, stress-relieving annealed at 400°C).

As shown by numerous studies [31, 32], plastic deformation in quasi-crystals is carried out by the movement and multiplication of dislocations, however, this mechanism manifests itself at temperatures above $(0.7-0.8)T_{melt}$ [5]. In a complex lattice of quasi-crystals, the activation energy of dislocation motion is very high (on the order of several eV [31]), and the temperature dependence of the yield stress is very sharp. Therefore, at low temperatures quasi-crystals do not exhibit microplasticity. For Al−Cu−Fe quasi-crystals, the critical temperature forbidding microplasticity is below 600°C. The fracture toughness of the Al−Cu−Fe quasi-crystal was estimated as $K_{1C} = (1.7 \pm 0.2)$ MPa·m$^{1/2}$ (at the ceramic level), but the presence of the I phase in Al−Cu−Fe alloys containing the λ phase and Θ phase changed the character fracture from a brittle cleavage to a quasi-cleavage [4].

Figure 9 shows the microscopic images of the fracture surface of the tensile sample of QC coating. Optical micrograph (Fig. 9, *a*) shows that the fracture surface is relatively uniform. SEM images confirm that intercrystallite fracture is the main type of the destruction process of the QC coating. Moreover, the residual pores mainly remain nearby the intergranules areas after formation of HVAF coating appears to has only a little influence (Fig. 9, *b*, *c*).

The optical images describing the surface morphologies of the studied Al$_{63}$Cu$_{25}$Fe$_{12}$ coatings containing 75% wt. of the quasi-crystalline
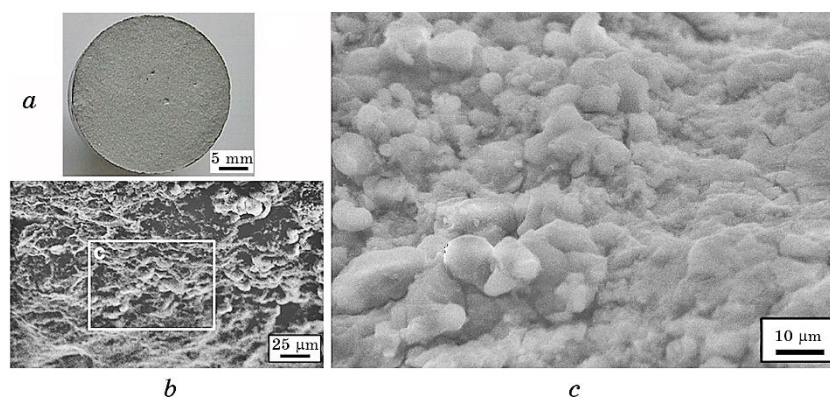
Fig. 9. Fracture surface of the tensile sample of QC containing coating on low-carbon steel substrate.
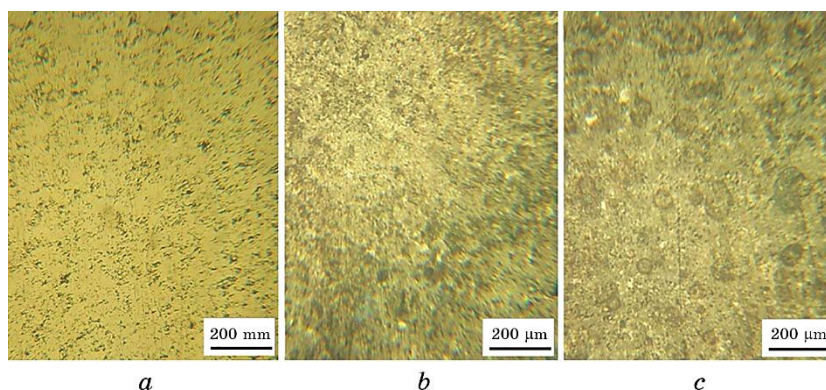
Fig. 10. Optical images of the QC containing coating surface in the as-coated state (*a*) and after holding in artificial sea-water (3% NaCl) for 3 days (*b*) and for 10 days (*c*) resulting in the formation of passive film.

phase after corrosion tests in a 3% NaCl solution (artificial sea water) for various holding times are shown in Fig. 10. After exposure to aggressive medium, the studied coating became darker, but no corrosion damage appeared on the coating surface. A metallographic study of the surface of the thin section of the coating showed that it is covered with a protective passivating film.

The study of corrosion properties of coatings should include the analysis of a number of factors, namely: surface roughness of the coating, its open porosity, the presence of phases of different chemical composition and the length of interphase boundaries, as well as residual elastic stresses in the coating [33, 34]. The electrochemical process of corrosion in electrolytes is very complex, it includes the selective dissolution of various elements and the formation of new phases on the surface, in particular oxide phases, which can create a strong passivating film.

Researches dwelt with the evaluation of corrosion behaviour of quasi-crystals based on the Al–Cu–Fe system are relatively rare. For example, the behaviour of quasi-crystalline $Al_{63}Cu_{25}Fe_{12}$ ingots was studied in comparison with different crystalline phases of the Al–Cu–Fe system, and this comparison was performed in alkaline and acidic solutions in the range of pH values of the hydrogen index from 0 to 13 [35]. In particular, as established, the corrosion resistance of the cast alloy is significantly higher than that of coatings made of it due to the greater perfection of the cast, and the significant difference in the chemical composition of the β and λ phases from the quasi-crystalline and/or approximant phase causes galvanic effects at the interphase boundaries and, accordingly, worsens the corrosion resistance. As suggested, the increased corrosion resistance of the decagonal quasi-

crystalline phase compared to the icosahedral phase is also of great importance [36]. However, the authors of the work [35] believe that the quasi-crystalline nature of the packing of atoms in the $Al_{63}Cu_{25}Fe_{12}$ lattice does not affect the corrosion properties of the $Al_{63}Cu_{25}Fe_{12}$ ingot, as they are very similar to the properties of the crystalline Al_7Cu_2Fe intermetalide of similar composition.

In our case, the main factor that determines corrosion resistance is the rapid formation of a passivation oxide film. Copper is known to increase the corrosion resistance of aluminium alloys as an electropositive metal, while iron, having a fairly high standard electrode potential, *i.e.,* not a very strong tendency to dissolve in general, exhibits strong pitting corrosion in an environment with Cl- ions. The formed passivation film mainly contains aluminium oxide. Aluminium, although it is an electronegative metal, has a very high tendency to passivation in this solution, in the series of passivities it stands directly behind titanium along with chromium [34]. The corrosion process is limited by the diffusion of oxygen dissolved in the electrolyte to the surface of the metal. The passivating oxide formed on aluminium has low electronic conductivity. It almost completely inhibits not only the anodic reaction of metal dissolution, but also the cathodic reduction of oxygen dissolved in the electrolyte.

4. CONCLUSIONS

This study shows a good efficiency of the method of high-velocity oxygen fuel spraying of water-atomized quasi-crystalline powders of the Al−Cu−Fe system on a low-carbon steel substrate in the production of protective coatings with sufficiently high mechanical characteristics and anti-corrosion properties.

It has been established that the HVAF spraying process allows producing the coating with controllable volume fraction of $Al_{63}Cu_{25}Fe_{12}$ quasi-crystalline phase, varied thickness and acceptable porosity. The produced QC coating possesses a high cohesion strength (~ 565 MPa) and good adhesion to the steel substrate providing avoidance of the coating detachment at bending.

A study of the behaviour of the $Al_{63}Cu_{25}Fe_{12}$ quasi-crystalline coating in artificial sea water showed its satisfactory resistance to the formation of surface corrosion damage due to the formation of a passivating oxide film based on aluminium oxide.

taining HVAF coatings.

REFERENCES

1.   J.-M. Dubois, *Mater. Sci. Eng. A*, **294–296**: 4 (2000).
2.   E. Huttunen-Saarivirta, *J. Alloys Compounds*, **363**: 150 (2004).
3.   H. R. Leonard, S. Rommel, T. J. Watson, T. Policandriotes, and M. Aindow, *Mater. Des.*, **182**: 108094 (2019).
4.   U. Köster, W. Liu, H. Liebertz, and M. Michel, *J. Non-Cryst. Solids*, **153–154**: 446 (1993).
5.   Yu. V. Milman, *Mater. Sci. Forum*, **482**: 77 (2005).
6.   M. Galano, F. Audebert, A. Garcia Escorial, I. C. Stone, and B. Cantor, *Acta Mater.*, **57**: 5120 (2009).
7.   S. M. Lee, J. H. Jung, E. Fleury, W. T. Kim, and D. H. Kim, *Mater. Sci. Eng. A*, **294–296**: 99 (2000).
8.   G. Laplanche, A. Joulain, J. Bonneville, R. Schaller, and T. El Kabir, *J. Alloys Compounds*, **493**: 453 (2010).
9.   B. N. Mordyuk, M. O. Iefimov, G. I. Prokopenko, T. V. Golub, and M. I. Danylenko, *Surf. Coat. Technol.*, **204**: 1590 (2010).
10. W. Wolf, L. C. R. Aliaga, D. N. Travessa, C. R. M. Afonso, C. Bolfarini, C. S. Kiminami, and W. J. Botta, *Mater. Res.*, **19**: 74 (2016).
11. B. N. Mordyuk, G. I. Prokopenko, Y. V. Milman, M. O. Iefimov, and A. V. Sameljuk, *Mater. Sci. Eng. A*, **563**: 138 (2013).
12. B. N. Mordyuk, G. I. Prokopenko, Y. V. Milman, M. O. Iefimov, K. E. Grinkevych, A. V. Sameljuk, and I. V. Tkachenko, *Wear*, **319**, Iss. 1–2: 84 (2014).
13. D. J. Sordelet, M. J. Kramer, and O. Unal, *J. Thermal Spray Technol.*, **4**: 235 (1995).
14. D. J. Sordelet, M. F. Besser, and L. E. Anderson, *J. Thermal Spray Technol.*, **5**: 161 (1996).
15. E. Fleury, S. M. Lee, W. T. Kim, and D. H. Kim, *J. Non-Cryst. Solids*, **278**: 194 (2000).
16. V. N. Balbyshev, D. J. King, A. N. Khramov, L. S. Kasten, and M. S. Donley, *Thin Solid Films*, **447–448**: 558 (2004).
17. M. Cekada, P. Panjan, D. Juric, J. Dolinsek, and A. Zalar, *Thin Solid Films*, **459**: 267 (2004).
18. M. O. Iefimov, D. V. Lotsko, Yu. V. Milman, A. L. Borisova, S. I. Chugunova, Ye. A. Astakhov, and O. D. Neikov, *High Temp. Mater. Proc.*, **25**: 31 (2006).
19. Yu. V. Milman, D. V. Lotsko, S. N. Dub, A. I. Ustinov, S. S. Polishchuk, and S. V. Ulshin, *Surf. Coat. Technol.*, **201**: 5937 (2007).
20. S. Yin, Q. Bian, L. Qian, and A. Zhang, *Mater. Sci. Eng. A*, **465**: 95 (2007).
21. F. Turquier, V. D. Cojocaru, M. Stir, R. Nicula, and E. Burkel, *J. Non-Cryst. Solids*, **353**: 3417 (2007).
22. O. D. Neikov, *Proc. of 2000 Powder Metallurgy World Congress (Nov. 12–16, 2000)* (Kyoto: Japan Society of Powder Metallurgy: 2000), p. 464.
23. O. D. Neikov, S. S. Naboychenko, I. B. Murashova, and N. A. Iefimov, *Handbook of Non-Ferrous Metal Powders* (Ed. O. D. Neikod) (Amsterdam: Elsevier: 2019), p. 685.
24. N. A. Iefimov, Powders with Quasicrystalline Structure, *Handbook of Non-*

Ferrous Metal Powders (Ed. O. D. Neikod) (Amsterdam: Elsevier: 2019), p. 313.

25. R. Nicula, F. Turquier, M. Stir, V. Y. Kodash, J. R. Groza, and E. Burkel, *J. Alloys Compounds*, **434−435: 319 (2007)**.
26. H. R. Leonard, S. Rommel, T. J. Watson, T. Policandriotes, and M. Aindow, *Mater. Des.,* **182: 108094 (2019)**.
27. Z. Bergant, U. Trdan, and J. Grum, *Corrosion Sci.,* **88: 372 (2014)**.
28. B. N. Mordyuk, G. I. Prokopenko, K. E. Grinkevych, N. A. Piskun, and T. V. Popova, *Surf. Coat. Technol.,* **309: 969 (2017)**.
29. L. Zhu, S. Soto-Medina, W. Cuadrado-Castillo, R. G. Hennig, and M. V. Manuel, *Mater. Des.,* **185: 108186 (2019)**.
30. Yu. M. Podrezov, Yu. V. Milman, Ya. I. Evich, M. O. Efimov, N. P. Korzhova, T. M. Legka, V. M. Kisel, Yu. I. Evdokimenko, and V. Kh. Melnik, *Electron Microscopy Strength Mater.*, **19**: 44 (2013) (in Russian).
31. M. Feuerbacher, C. Metzmacher, M. Wollgarten, K. Urban, B. Baufeld, M. Bartsch, and U. Messerschmidt, *Mater. Sci. Eng. A,* **233: 103 (1997)**.
32. E. Giacometti, P. Guyot, N. Baluc, and J. Bonneville, *Mater. Sci. Eng. A,* **319−321: 429 (2001)**.
33. V. N. Balbyshev, D. J. King, A. N. Khramov, L. S. Kasten, and M. S. Donley, *Thin Solid Films,* **447−448: 558 (2004)**.
34. C. Zhou, R. Cai, S. Gong, and H. Xu, *Surf. Coat. Technol.,* **201: 1718 (2006)**.
35. A. Rüdiger and U. Köster, *Mater. Sci. Eng. A,* **294−296: 890 (2000)**.
36. V. A. Polonskyy, O. V. Sukhova, and V. A. Ivanov, *J. Chem. Technol.,* **30,** No. 2: 166 (2022).